Mapping Ligand Interactions with the Hyperpolarization Activated Cyclic Nucleotide Modulated (HCN) Ion Channel Binding Domain Using a Soluble Construct†

Sean-Patrick Scott,*,‡ Patrick W. Shea,§ and Stuart E. Dryer||

Escuela de Medicine, Tec de Monterrey, Edificio CITES 3er piso, Área de Investigación, Av. Morones Prieto 3000 Pte., Col. Los Doctores, Monterrey, N.L. 64710, México, University of Texas Medical School, Houston, Texas 77030, and Department of Biology and Biochemistry, University of Houston, Houston, Texas 77204

Received December 19, 2006; Revised Manuscript Received June 7, 2007

ABSTRACT: Hyperpolarization activated cyclic nucleotide modulated (HCN) ion channel currents are activated by hyperpolarization and modulated in response to changes in cytosolic adenosine 3′,5′-cyclic monophosphate (cAMP) concentrations. A cDNA chimera combining the rat HCN2 cyclic nucleotide binding domain and the DNA binding domain of the cAMP receptor protein (CRP) from *E. coli* and the histidine tag (HCN2/CRP) was expressed and purified. The construct is capable of forming only non-ligand dependent dimers because the C-linker region of the channel is not present in this construct. The construct binds 8-[[2-[(fluoresceinylthioureido) amino] ethyl] thio] adenosine-3′,5′-cyclic monophosphate (8-fluo cAMP) with a K_d of 0.299 μM as determined with a monomer binding model. The K_i values of 20 ligands related to cAMP were measured in order to determine the properties necessary for a ligand to bind to the HCN2 binding domain. This is the first report of cAMP and gunaosine 3′,5′-cyclic monophosphate (cGMP) affinities to the HCN2 binding domain being equivalent, even though they modulate the channel with a 10-fold difference in $K_{0.5}$. Furthermore, the array of ligands measured allows the preference rank order for each purine ring position to be determined: position 1, H > NH_2 > O; position 2, NH_2 > Cl > H > O; position 6, NH_2 > Cl > H > O; and position 8, NH_2 > Cl > H > O. Finally, the ability of HCN2/CRP to bind cyclic nucleotide pyrimidine rings at concentrations approximately 1.33 times greater than cAMP suggests that ribofuranose is key for binding.

A functional understanding of ligand gated ion channels depends on the ability to distinguish between ligand binding to and ligand activation of, or gating of, the ion channel (*1*). Current maxima (I_{max}) and apparent affinities represented by half activation ($K_{0.5}$) can give information about the ability of a ligand to activate and lead to assumptions about how ligands bind and activate the channel. In the end, however, they are only assumptions. The goal of this research is to separate channel activation from ligand binding for a class of ligand modulated ion channels. By understanding the ability of different ligands to bind to the binding domain in the absence of other parts of the channel, the binding energy for ligand only can be determined without concern for the reciprocity of other portions of the channel and the energy dissipated or used in channel activation. Hence, only ligand binding is determined, and the amount of energy available for channel activation can be determined. Here, we introduce a binding assay that gives binding in terms of K_i for a wide array of ligands.

The existence of the hyperpolarization activated cyclic nucleotide modulated (HCN[1]) ion channel was first found (*2*) and characterized (*3*) in sino-atrial node tissue as inward current that was activated by membrane hyperpolarization, called $I_{h(yperpolarization)}$ (or $I_{f(unny)}$). Similar current was then identified in hippocampal pyriamidal neurons (*4*) and rod photoreceptors (*5*) and called $I_{Q(ueer)}$. At least four physi-

† This work was supported by American Heart Association Scientist Development Grant, 0230378N.

* Corresponding author. Phone: 011-52-81-8888-2105. Fax: 011-52-81-8143-0108. E-mail: sscott04@msn.com.

‡ Escuela de Medicine.

§ University of Texas Medical School, Houston.

|| University of Houston.

[1] Abbreviations: HCN, hyperpolarization activated cyclic nucleotide modulated ion channel; CRP, cAMP receptor protein; CAP, catabolite gene activating protein; CNG, cyclic nucleotide gated ion channel; Rp-cAMPS, adenosine-3′,5′-monophosphorthioate, Rp-isomer; Sp-cAMPS, adenosine-3′,5′-monophosphorothiate, Sp-isomer; cCMP, cytidine-3′,5′-monophosphate; 6-Cl-cPMP, 6-chloropurine riboside-3′,5′-cyclic monophosphate; cPMP, purine-1-β-D-ribofuranoside-3′,5′-cyclic monophosphate; cUMP, uridine-3′,5′-cyclic monophosphate; 8-MA-cAMP, 8-methylaminoadenosine-3′,5′-cyclic monophosphate; 2-Cl-cAMP, 2-chloroadenosine-3′,5′-cyclic monophosphate; cXMP, xanthosine-3′,5′-cyclic monophosphate; 8-Cl-cAMP, 8-chloroadenosine-3′,5′-cyclic monophosphate; 2′-O-Me-cGMP, 2′-*O*- methylguanosine-3′,5′-cyclic monophosphate; 1-NH_2-cGMP, 1-aminoguanosine-3′,5′-cyclic monophosphate; Sp-cAMPS-AM, adenosine-3′,5′-cyclic monophosphate, Sp-isomer, acetoxymethyl ester; NO-cAMP, adenosine-N^1-oxide-3′,5′-cyclic monophosphate; 2′-O-MB-cAMP, 2′-*O*-monobutyryladeonsine-3′,5′-cyclic monophosphate; 2-NH_2-PMP, 2-aminopurine riboside-3′,5′-cyclic monophosphate; 8-OH-cAMP, 8-hydroxyadenosine-3′,5′-cyclic monophosphate; 8-fluo-cAMP, 8-[[2-[(fluoresceinylthioureido) amino] ethyl] thio] adenosine-3′,5′-cyclic monophosphate; 8-fluo-cGMP, 8-[[2-[(fluoresceinylthioureido) amino] ethyl] thio] guanosine-3′,5′-cyclic monophosphate; cAMP, adenosine 3′,5′-cyclic monophosphate; cGMP, guanosine 3′,5′-cyclic monophosphate.

10.1021/bi6026049 CCC: $37.00
Published on Web 07/26/2007

ological roles have been attributed to I_h: (1) control of pacemaker activity in the heart and brain, (2) regulation of resting potential, (3) control of membrane resistance and dendritic integration, and (4) regulation of synaptic transmission (*6*). Four subtypes of HCN have been cloned (*7*, *8*) with varying tissue localization. These channels are related to the cyclic nucleotide gated (CNG) channel family by structural homology, even though the gating mechanism of the two channels differ, one relying on voltage and modulated by ligand and the other solely on ligand activation (*9*). A functional channel takes four subunits to work with each subunit coming from a single transcript. Each transcript contains 6 transmembrane helices, a pore region between transmembrane helices 5 and 6, the voltage sensor being the fourth helix, an N-terminal region, and a C-terminal region which contains the cyclic nucleotide binding domain and C-linker region (*9*). The cyclic nucleotide binding domain used in this series of experiments is taken from the rat HCN type 2. The modulation of HCN2 by cAMP occurs with a $K_{0.5}$ of 0.5 μM, which is roughly an order of magnitude lower in concentration than the $K_{0.5}$ of cGMP of 6 μM (*8*).

Crystal structures of the HCN2 cyclic nucleotide binding domain interacting with either cAMP or cGMP suggest that the following residues are important for ligand binding and channel activation: residues Gly 581 (construct number 88), Glu 582 (89), Cys 584 (91), Arg 591(98), and Thr 592 (99), with the ribofuranose. Residue Arg 632 (139) positioning Glu 582 via a charge−charge interaction and with *anti*-cAMP via the residue's backbone nitrogen. Hydrophobic residues that interact with the purine ring are Val 564 (71), Met 572 (79), Leu 574 (81), and Ile 636 (143) (*10*). There are three crystal structures available in the protein database for the HCN2 binding domain. Two were used in molecular modeling, 1Q5O, which binds *anti*-cAMP, and 1Q3E, which binds *syn*-GMP.

The major difference we are concerned with between these structures, other than containing different ligands, is the position of β-strands 4 and 5 and B and C α-helices. All the other heavy atoms in the β-barrel of the binding domain line up within the error of the structures. The other major difference between these structures is the quaternary structure of the binding domains. A dimer is formed between the large helix of each binding domain in an antiparallel configuration with the C-linker region faced away from the dimerization area with cGMP bound in pdb file 1Q3E. A tetramer is formed between the cAMP-bound binding domains using the C-linker region as the tetramerization domain in pdb file 1Q5O. We are not concerned with any higher order multimerization other than a dimer because our construct lacks the C-linker region altogether.

The interactions that occur in the soluble constructs are thought to necessarily occur in the complete channel with respect to the bound ligand. A growing sense is that the tertiary structure of the cAMP-bound binding domain as suggested by the HCN2 crystal structures may be the closed conformation (*11*). The structurally homologous CNGC binding domain from *M. loti* crystallizes with the binding domains in different orientations altogether and may represent the open conformation with A α-helices interacting between two binding domains (*12*). What will not change is the ability of the ligand to take different conformations and interact with surrounding amino acids, even though the role of the tertiary structure of the binding domain may be questionable.

The ability of the ligand to bind is defined by the amino acids that line the binding domain region. It is these amino acids that define the interactions, the energy available for other activities in the channel, and what ligands are capable of binding to the channel. It is for this reason that we designed a construct to measure the binding of many different ligands to determine the ability of the ligand to bind to the ion channels binding domain. If the ligand cannot bind to the binding domain alone, then logically, it is unable to bind to a complete channel and modulate or activate current. If, however, the ligand is capable of binding to the binding domain but shows varied channel activation, this is due to the way in which the binding domain communicates with the ligand and then transfers that information to the rest of the protein.

We made a soluble construct by replacing the binding domain of the cAMP receptor protein (CRP or CAP, catabolite gene activating protein) with that of the HCN ion channel. CRP is a soluble 209 amino acid (*13*−*15*) transcription factor from *Escherichia coli* that binds cAMP and cGMP with similar affinity but is activated only by cAMP (*16*). Each subunit contains an N-terminal cyclic nucleotide binding domain and a C-terminal DNA binding domain. The CRP cyclic nucleotide binding domain was the first member of this family whose structure was determined (*17*) and has defined the cyclic nucleotide binding domain, an eight stranded β-barrel preceded by a single α-helix and followed by two α-helices. There are two conserved glycines (560 and 581 in HCN2 binding domain) that are important for maintaining the fold of the barrel (*18*) as well as conserved Glu (582) and Arg (591) residues that interact with the cyclic nucleotide ribofuranose and are important for binding the ligand (*19*, *20*). This construct is similar to that used to measure cAMP and cGMP binding in a soluble cyclic nucleotide gated (CNG) channel cyclic nucleotide binding domain (*21*). The measurements differ in using a fluorescent probe that allows for measurement of ligands that do not have radioactive analogues.

Herein, we look at a series of 20 ligands in order to map interactions between ligand and the HCN2 cyclic nucleotide binding domain. Thirteen of these ligands, including cAMP and cGMP, have variations in the purine ring, 5 have changes in the ribofuranose, and 2 replace the purine ring with a pyrimidine ring. Each of these ligands has two components, a ribofuranose and a purine or pyrimidine ring. The ribofuranose defines the ability of the ligand to bind, and alterations made to it can result in a loss of binding. The second component is the purine or pyrimidine ring, which modulates the ability of the ligand to bind. By making modification to the ribofuranose or ring, we explored the ability of the HCN2 binding domain to bind various ligands and refine the amino acids with which the ligand binds.

MATERIALS AND METHODS

Ligands. The ligands used in this study from Biolog Life Science Institute are as follows (format: name (abbreviated name) (catalog number)): adenosine-3′5′-monophosphorthioate, Rp-isomer (Rp-cAMPS) (A 002 S); adenosine-3′,5′-monophosphorothiate, Sp-isomer (Sp-cAMPS) (A 003 S);

cytidine-3′,5′-monophosphate (cCMP) (C001); 6-chloropurine riboside-3′,5′-cyclic monophosphate (6-Cl-cPMP) (C 002); purine-1-β-D-ribofuranoside-3′,5′-cyclic monophosphate (cPMP) (P010); uridine-3′,5′-cyclic monophosphate (cUMP) (U 001); 8-methylaminoadenosine-3′,5′-cyclic monophosphate (8-MA-cAMP) (M001); 2-chloroadenosine-3′, 5′-cyclic monophosphate (2-Cl-cAMP) (C 020); xanthosine-3′,5′-cyclic monophosphate (cXMP) (X 001); 8-chloroadenosine-3′,5′-cyclic monophosphate (8-Cl-cAMP) (C 007); 2′-*O*-methylguanosine-3′,5′-cyclic monophosphate (2′-O-Me-cGMP) (M 036); 1-aminoguanosine-3′,5′-cyclic monophosphate (1-NH_2-cGMP) (A 041); adenosine-3′,5′-cyclic monophosphate, Sp-isomer, acetoxymethyl ester (Sp-cAMPS-AM) (A 035); adenosine-N^1-oxide-3′,5′-cyclic monophosphate (NO-cAMP) (A023); 2′-*O*-monobutyryladeonsine-3′,5′-cyclic monophosphate (2′-O-MB-cAMP) (M 007); 2- aminopurine riboside-3′,5′-cyclic monophosphate (2-NH_2-PMP) (A 027); 8-hydroxyadenosine-3′,5′-cyclic monophosphate (8-OH-cAMP) (H 003), and 8-[[2-[(fluoresceinylthioureido) amino] ethyl] thio] adenosine-3′,5′-cyclic monophosphate (8-fluo-cAMP) (F002). The following ligands were obtained from Sigma-Aldrich: adenosine-3′,5′-cyclic monophosphate sodium salt monohydrate (cAMP) (A6885) and gunaosine-3′,5′-cyclic monophosphate sodium salt (cGMP) (G6129).

Protein Construction. The clones used for construction of HCN2/CRP were CRP in vector pET28a (Novagen) and a fragment of the HCN2 channel in pCR 2.1- TOPO cloning vector. The PCR methods of gene splicing by overlap extension (*22*) were used to add the CRP N-terminus and DNA-binding domain to the cyclic nucleotide binding domain of HCN2 and mutate SER 128 in CRP to ALA. The constructs were sequenced after cloning into the pET28a vector from both the 5′- and 3′-ends. The first round of PCR joined the N-terminal CRP fragment with HCN2 using the T7 promoter of pET28a, internal primers linking the CRP N-terminal to the HCN2 binding domain N-terminal region, GCAAACAGACCCCAACTTCGTC and AGTTGGGGTCTGTTTGCGGTTT, and a C-terminal primer which was used to mutate SER 128 and join the HCN2 binding domain C-terminus to the DNA binding domain, CTTTCTCTGCTATGCGGTCCAGA-CGGT. The full PCR fragment was produced using the two external primers of T7 and the C-terminal primer. A third DNA fragment was produced using the complimentary C-terminal primer, ACCGCATAGCAGAGAAAGTGGGCAAC, and T7 reverse primer on the CRP pET28a clone. The T7/C-terminus fragment and the third fragment were combined with the external primers of T7 and T7 reverse primers to produce the full construct. The construct was restricted with Nde I and Ecor I and placed into fresh pET 28a vector.

Expression and Purification. HCN2/CRP containing His· Tags were expressed in the IPTG-inducible vector pET 28a in BL21 (DE3) Lys S cells at 37 °C from Novagen. Four liters of LB media were allowed to grow to an OD_{600} of ~0.8 when 0.24 g/L IPTG was added. The temperature was decreased to 25 °C in a refrigerated shaking incubator (Model # SHKA 4000-7 manufactured by Barnstead/Lab-Line). The cells were allowed to grow for an additional 5 h before harvesting. The cells were centrifuged at 3,000 rpm for 30 min in a refrigerated centrifuge (Hermle Z383K, distributed by Labnet International Inc.), with a CO383-75 swing out rotor. The pellets were resuspended in PC buffer at pH 7.4. The slurry was sonicated with a sonic dismembrator (Model 500 manufactured by Fisher Scientific) 6 times with a duty cycle of 1 min on and 1 min off, with an amplitude 40% on ice. The resultant mixture was centrifuged at 12,000 rpm in a CO382-91 angel rotor at 8 × 50 mL at 4 °C. The supernatant was combined and dialyzed against a purification buffer (50 mM Tris at pH 7.4, 0.1 M NaCl, 2 mM EDTA, 1 mM β-mercapto ethanol, and 5% glycerol) before loading onto ~20 mL of BioRex 70 ion-exchange resin. Up to 12 L of bacteria grown over 3 days were combined for a single purification.

The Bio-Rex 70 column was washed with ~100 mL of buffer and eluted with a salt gradient from 100 mM to 2 M NaCl in PC buffer, collecting 5 mL fractions for a total gradient of 150 mL. All purifications and dialysis were carried out at 4 °C. The fractions were analyzed by SDS−PAGE and Western blotting. Fractions were selected for purity and quantity of HCN2/CRP. Selected samples were dialyzed into Ni^{2+} column binding buffer (20 mM Tris (pH 7.9), 0.5 M NaCl, 0.1% Triton X 100, and 5 mM imidazole) and bound to a Ni^{2+} column. Approximately 12.5 mL of Ni^{2+} agarose resin from Novagen was charged and prewashed with binding buffer before the protein was batch-loaded onto the column. The column was washed with 120 mL of binding buffer, followed by 80 mL of wash buffer (20 mM Tris (pH 7.9), 0.5 M NaCl, 0.1% Triton X 100, and 60 mM imidazole). The protein was released from the column in a step with elution buffer (20 mM Tris (pH 7.9), 0.5 M NaCl, 0.1% Triton X 100, and 1 M imidazole) in 5 mL fractions. Fractions were again selected for purity and amount via SDS−Page and Western blotting, combined, and dialyzed into working buffer (20 mM Tris (pH 7.9), 0.5 M NaCl, 1 mM EDTA, 1 mM β-mercaptoethanol, and 0.1% Triton X 100). Typically, selections of Ni^{2+} column samples were made within 24 h and in no more than 72 h. Final protein concentration was determined using SDS−PAGE gels and running varying amounts of protein (1−25 μL) with fixed amounts of LMW Calibration Kit for SDS Electrophoresis (Amersham Pharmacia Biotech UK Limited).

Transblotting. Transblotting was performed per the instructions of the Panther Semidry Electroblotter, model HEP-1, Owl Separation Systems. Briefly, a recently run SDS−PAGE gel was placed on wet transblot paper (Whatman gel blot paper, GB 004, from Schleicher & Schuell) with transblot buffer (25 mM Tris, 200 mM Glycine, and 20% v/v Methanol), a sized piece of Whatman Protran 0.45 μm Nitrocellulose membrane, BA 85, from Schleicher & Schuell was placed on top of the gel, followed by a final piece of transblot paper. The transblot was typically finished within 2 h. The gel was Coomassie stained to ensure that transfer was complete. The transblot was then washed in blocking buffer (50 mM Tris at pH 7.4, 200 mM NaCl, 0.1% v/v Tween 20, and 5% w/v Carnation Instant Nonfat Dry Milk) for at least 1 h before 1:1000 His·Tag antibody (His·Tag Monoclonal Antibody from Novagen, Cat #. 70796-3) resuspended in water in blocking buffer was added for an hour. The blot was then washed 3 times for 10 min with wash buffer (50 mM Tris at pH 7.4, 200 mM NaCl, and 0.1% v/v Tween 20). The transblot with primary antibody was then mixed with 1:1000 secondary antibody (Anti-Mouse IgG (H&L) HRP Linked Antibody from Cell Signaling, Cat # 7076) in blocking buffer for 1 h. This was washed 3 times

with wash solution for 10 min. The secondary antibody was labeled using Super Signal West Pico Chemiluminescent Substrate by Pierce, product number 34080. Equal amounts of SuperSignal West Pico Stable Peroxide Solution and SuperSignal West Pico luminol/Enhnacer solution were mixed to make typically a 1 mL solution. The blot was placed face down onto this solution for 5 min and then dabbed with a paper towel to remove excess solution. X-ray film was placed onto the blot for 1−30 s before being developed with a Kodak Processor (Model M7B).

Fluorescence Binding Experiments. Fluorescence binding experiments of 8-fluo-cAMP (BioLog, La Jolla, CA) and HCN2/CRP were carried out at 20 °C using an ISS OC spectrofluorimeter (ISS, INC. Champaign, IL). The excitation wavelength was 480 nm and the emission 540 nm. The protein and 8-fluo-cAMP were mixed in a cuvette with a total volume of 200 μL. Following each measurement, an aliquot was removed and then replaced with the ligand solution to keep the ligand concentration fixed while decreasing the protein concentration. Polarization was measured after equilibration following each addition, typically after 90−120 s. A 1-site binding model was used to fit these data with protein expressed as monomer concentrations. Attempts to use 8-fluo-cGMP as a probe failed as there was minimal increase in polarization at high protein concentrations.

Determination of K_d. Determination of K_d was performed by normalizing all of the protein binding curves generated throughout the experiments into a single curve. The single curve was fit to the following single binding site series of equations:

$$K_d = ([L]_0 \times [P]_0)/[PL]_0$$

$$[L]_{Total} = [L]_0 + [PL]_0$$

$$[P]_{Total} = [P]_0 + [PL]_0$$

$$\rho_{Total} = \rho_{bound}([PL]_0/[L]_{Total}) + \rho_{free}([L]_0/[L]_{Total}) \quad (1)$$

where $[PL]_0$ is the bound ligand, K_d is the binding constant, $[L]_{Total}$ is the total concentration of ligand, $[P]_{Total}$ is the total concentration of protein binding sites, $[L]_0$ is the free ligand, $[P]_0$ is the free protein, ρ_{bound} equaled the maximum polarization when all protein is bound, ρ_{free} the associated polarization when ligand is not bound, and ρ_{Total} is the polarization measured. The resulting polynomial was solved for $[PL]_0$ as follows:

$$[PL]_0^2 - (K_d + [P]_{Total} + [L]_{Total}) \times [PL]_0 + ([P]_{Total} \times [L]_{Total}) = 0$$

using an assumed K_d and taking the negative root to calculate ρ_{Total}. The least squares method was used to determine the best K_d to fit the measured ρ_{Total}. The ρ_{bound} and ρ_{free} values used were 0.32 and 0.074, respectively.

Competition Binding Experiments. Competition binding experiments were carried out by mixing an inhibitor (for example cAMP), 8-fluo-cAMP, and HCN2/CRP in a 200 μL cuvette. An aliquot was removed and then replaced with a fixed concentration of protein and 8-fluo-cAMP effectively decreasing the inhibitor concentration. The polarization measurement was taken after 2 min. The method derived by Nikolovska-Coleska et al. (*23*) was used to determine the K_i of each inhibitor. Briefly, the following equation was used to determine K_i:

$$K_i = [I]_{50}/([L]_{50}/K_d + [P]_0/K_d + 1) \quad (2)$$

where $[I]_{50}$ is the concentration of free inhibitor at 50% inhibition, $[L]_{50}$ is the concentration of the free 8-fluo-cAMP at 50% inhibition, $[P]_0$ is the concentration of free protein at 0% inhibition, and K_d is the concentration of the free protein−ligand complex. K_d was calculated from the protein binding experiments, and $[P]_0$ is easily calculated with known $[P]_{Total}$ and $[PL]_0$. The $[L]_{50}$, the concentration of 8-fluo-cAMP at half inhibition, can be easily calculated from the known variables by the following equation:

$$[L]_{50} = [L]_{Total} - [PL]_0/2$$

IC_{50}, concentration of inhibitor at half inhibition, is calculated from an inhibition curve by fitting the following relationship:

$$\rho = ((\rho_{maximum} - \rho_{minimum})/(1 + ([I]_{Total}/IC_{50}))) + \rho_{minimum}$$

where $[I]_{Total}$ is the total concentration of inhibitor. Once the IC_{50} is known, the $[I]_{50}$ can be calculated from the following equation:

$$[I]_{50} = IC_{50} - [P]_{Total} + K_d([PL]_0/2)/\ [L]_{50} + ([PL]_0/2) \quad (3)$$

where all of the variables have been previously defined. The variables in eq 2 are replaced by known values, and the K_i for each inhibitor, or ligand, is now known.

Molecular Models. Molecular models were made of the HCN2/CRP construct from two starting templates, 1Q50 (monomer with cAMP) and 1Q3E (dimer with cGMP) (*10*). Five series of models were made with all of the purine ring ligands replacing the bound ligand. The *syn* conformation of cGMP from 1Q3E was used as the starting template for all *syn* ligands, and the *anti*-cAMP conformation of 1Q5O was used for all *anti* conformation purine ring ligands. These two structures were chosen because they best represented the two conformations of the C α-helix present in the series of structures when the available structures, 1Q3E, 1Q43, and 1Q5O, were aligned along the 8-stranded β-barrel. These two structures differ by having a different angle between the B and C α-helices, which propagates through the C α-helix.

Three models used 1Q3E as the starting template including a series with the construct as a dimer, the construct as a monomer, and then of the cyclic nucleotide binding domain alone as a monomer. The starting template removed all heavy atoms not present in the construct including the C-terminal region thought to be important for tetramerization. The A α-helix, the end of the C α-helix, and DNA binding domain from CRP (*24*, *25*) were added by using the template's heavy atoms to guide positioning. The DNA binding domain was put in an open position parallel to the cyclic nucleotide binding domain to mimic the likely early stages of CRP protein conformation (*26*). Selenomethionine residues were replaced with methionine. Two models used 1Q5O as the starting template including a series with HCN2/CRP as a

A.

```
1          11         21         31         41
                                 αA         β1
MGSSHHHHHH SSGLVPRGSH mvlgkpqtDP NFVTAMLTKL KFEVFQPGDY

51         61         71         81         91
β2         β3   β4         *β5   β6   #αP      #*
IIREGTIGKK MYFIQHGVVS VLTKGNKEMK LSDGSYFGEI CLLTRGRRTA

101        111        121        131        141
β7   β8    αB         αC   *    *
SVRADTYCRL YSLSVDNFNE VLEEYPMMRR AFETVAIDRL DRIaekvgnl

151        161        171        181        191
     αD         β9   β10   αE
aFldvtgria qtllnlakqp damthpdgmq ikitrqeigq ivgcsertvg

201        211        221
αF         β11  β12
rilkmledqn lisahgktiv vygtr
```

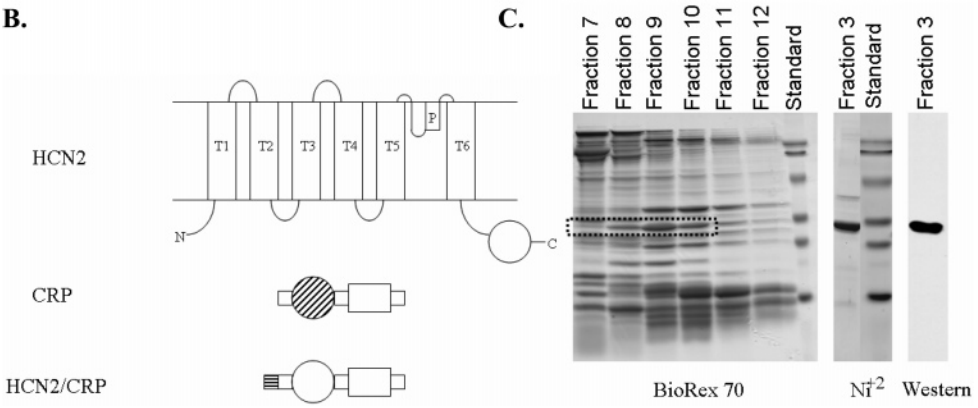

FIGURE 1: Producing a chimera containing the HCN2 cyclic nucleotide binding domain. (A) Sequence of the HCN2/CRP chimeric protein. The first 20 amino acids (*CAPITAL ITALICS*) represent the His·Tag added to ease purification. The next 8 and final 61 residues (lower case) represent CRP amino acids and include the CRP DNA binding domain. The middle amino acids (CAPITAL) are those of HCN2 cyclic nucleotide binding domain. The single mutation (*lower case italics*) was added to ensure that no contribution occurred from the CRP-like binding domain. The residues marked with * interact with the purine ring and those with # the bound cyclic nucleotide's ribofuranose. The structural elements for HCN2 were defined by the HCN crystal structure just as those of CRP were defined by the CRP crystal structure. (B) Scheme of the chimera. The cyclic nucleotide binding domain (circle) was taken from the rat HCN2 clone and replaced the equivalent binding domain (circle with stripes) in cAMP receptor protein (CRP). The CRP DNA binding domain was retained (large square), and a His·Tag was added for purification (small square with stripes). (C) Purification of the HCN2/CRP chimera. A two column approach was used. First, a BioRex 70 column at pH 9.0 was used to remove CRP contamination using differences in protein pI. Second, the fractions in the dotted box were run over the Ni^{2+} column to remove remaining contamination. A visible band just below the HCN2/CRP band would be apparent if there was greater than 5% CRP contamination. An antibody against the His·Tagged protein was used to ensure that the correct protein was purified.

monomer and the HCN2 cyclic nucleotide binding domain alone. The choice of models represents the complete construct as a possible dimer, as a monomer, and as that derived with the fewest additions from the structures available from the protein database. The models were minimized as described previously (*26*). Briefly, heavy atoms were fixed while missing, mostly hydrogen and differing ligand atoms, were minimized into position using AMMP (*27*). Once these were positioned, all atoms of the model were minimized until an energy minimum was reached. The models were visually checked for structural deformations, particularly the replaced ligands. The interaction energy of the ligand with the model was calculated for each ligand to see if it corresponded to binding order or could predict *anti* or *syn* conformation.

RESULTS

Construction of HCN2/CRP. The rat HCN2 subunit contains 834 amino acids (*28*), has large cytoplasmic domains on the N- and C-termini, 6 transmembrane regions, and a pore region between transmembrane 5 and 6 (see schematic in Figure 1B). The cyclic nucleotide binding domain is contained in a 115 amino acid stretch of the C-terminus. This is the general layout for all HCN/CNG channel family members, although the size of the cytoplasmic domains can vary. CRP contains a binding domain that has minimal, 22% identical, 39% homologous, sequence homology but high structural homology to the HCN2 binding domain. CRP contains a DNA binding domain in the C-terminus, which was combined with the HCN2 ligand binding domain. The

initial N-terminus of CRP was retained in order to provide for the initial fold of the protein. A His·Tag was added to the N-terminus in order to help purify the protein and provide a known epitope for antibody binding. The construct was created using PCR methods and was sequenced in order to check the fidelity of the sequence (see Figure 1A). In Figure 1, the initial His·Tag is in capital italic letters, the sequence derived from HCN2 is in capital letters, the CRP derived sequence is in lower case letters, and a mutation in either sequence is in lower case italic.

Expression and Purification of Soluble HCN2/CRP. The construct was produced under the T7 promoter of the pET28a vector in BL(21)DE3 cells (all from Novagen). The bacteria were grown, typically overnight, until the required absorption in 4 L when 200 mg/L of IPTG was added was reached and the cells allowed to grow for a further 5 h. The cells were collected via centrifugation, resuspended into buffer, and sonicated. The supernatant from a 30 min 14 K spin was retained and dialyzed into buffer at 4 °C. Up to three supernatants would be combined into a single batch before purification for a total of supernatant from 12 L of bacteria. No more than 3 days were allowed to pass from the production of the initial supernatant until loading the column. The supernatant was batch-loaded onto a BioRex70 column, washed, and then treated to a salt concentration gradient. Typical eluents are seen to the left of Figure 1C. The fractions containing the protein of interest (outlined with dotted box) were combined and dialyzed into buffer for purification by the His·Tag. Typically, most of the protein would come off the His·Tag column in a single eluent (middle of Figure 1C) with initial amounts in the preceding fraction and more tapering off. The protein was at least 95% pure as seen in this Figure. The protein was shown to be the construct by Western blotting (right of Figure 1C).

Fractions were collected and dialyzed into buffer for fluorescence assay. The typical yield was up to 20 mL of protein concentrated to no more than 0.2 mg/mL for a total of ~4 mg/12 L bacterial culture. Further concentrating the protein resulted in the formation of particulates. Once formed, the particulates would seed further rapid precipitation of the protein. The protein was therefore not concentrated further. The protein was stored at 4 °C at all times except when fluorescent experiments were conducted. The soluble construct was a dimer in solution (data not shown). Proteolytic cleavage assays showed minimal ligand dependence and showed a stable ~12 kDa protein (data not shown), which corresponds to a well folded ligand binding domain.

HCN2/CRP Binds 8-Fluo-cAMP. Each batch of ligand binding assays had at least one 8-fluo-cAMP curve run during the series of curves to obtain bound and free polarization, to ensure correct standardization of protein concentration, and to ensure a high signal-to-noise ratio. We decided to fit the curves as a single data set, even though each curve could be individually fit for K_d by the series of equations (eq 1). The reason for fitting the combined data set was to obtain a composite value for K_d using all the data points. The free and bound polarizations changed as the protein aged; therefore, all the curves were normalized to the curve with the best signal-to-noise ratio for polarization in order to produce Figure 2A. The bound polarization of this Figure is 0.32 with a free of 0.074 with an effective signal of 0.246. The range of bound polarizations for all curves was 0.227 to 0.34, and the free range was 0.074 to 0.115. In all curves used, the effective signal was greater than the free polarization, ranging from 0.111 to 0.256. The protein concentration was determined by running protein gels and estimating the concentration based on standards run using Scion imaging software by Scion Corp. The fit data had a K_d of 0.299 μM with an r^2 of 0.988. For completeness the data sets were fit by a Hill Equation. The individual data sets had a $K_{0.5} = 0.341$ μM with a standard deviation of 0.066 μM and an $N_h = 1.07 \pm 0.09$. The combined data set had a $K_{0.5} = 0.345$ μM with an $N_h = 1.04$ and an $r^2 = 0.988$.

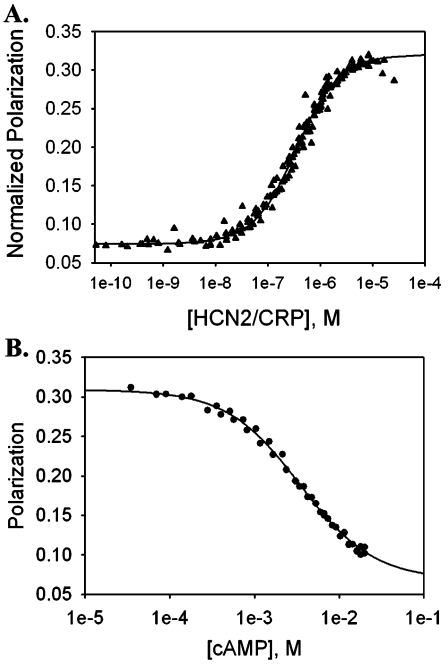

FIGURE 2: 8-Fluo-cAMP binding and competition curves. (A) Normalized polarization curve of all 8-fluo-cAMP curves fit to a single binding site model. The K_d for 8-fluo-cAMP is 0.299 μM with an $r^2 = 0.988$. (B) Competition curve of cAMP and HCN2/CRP with 8-fluo-cAMP and an $IC_{50} = 3.45$ mM with an $r^2 = 0.996$. The IC_{50} was used to determine the K_i of cAMP with 8-fluo-cAMP using the method of Nikolovska-Coleska et al. to be 60.8 μM.

Cyclic Nucleotide Inhibition Curves 8-Fluo-cAMP. Cyclic AMP competitively bound 8-fluo-cAMP in order to produce a competition curve (Figure 2B) with an $IC_{50} = 3.45$ mM and an $r^2 = 0.996$. The IC_{50} is meaningless without entering it into eq 3 and entering the corresponding result into eq 2 with the corresponding numbers for the batch. The following values were obtained: $IC_{50} = 3.45$ mM, $[L]_{50} = 50.9$ nM, $[P]_{Total} = 16.6$ μM, $[PL]_0 = 98.2$ nM, and $K_d = 0.299$ μM to give an $[I]_{50}$ of 3.43 mM with a $[P]_0 = 16.5$ μM. A result of $K_i = 60.8$ μM is obtained. This competition curve is made up of two data sets collected on the same batch of protein. All batches of protein had at least one ligand curve repeated from another batch so as to standardize all the curves. For example, when cAMP was run on a different batch of protein, the following results were obatined: $[IC]_{50} = 1.06$ mM, $[L]_{50} = 52.6$ nM, $[P]_0 = 5.53$ μM, and $K_d = 0.299$ μM, resulting in a $K_i = 53.8$ μM or $K_i = 57.3$ μM with a standard deviation of 5 μM over the two batches. Only select ligands were run on more than a single batch because of the limited amount of protein and ligand. Those ligands were 6 Cl-cPMP with $K_i = 103$ μM and SD = 23.5 μM, and cPMP with $K_i = 146$

Table 1: Purine Ring Substituent of Each Ligand and the Associated K_I[a]

ligand	1	2	6	8	K_i (μM)
cAMP		H	NH_2	H	57.3
NO-cAMP	O	H	NH_2	H	853
2-Cl-cAMP		Cl	NH_2	H	34.2
8-Cl-cAMP		H	NH_2	Cl	18
8-MA-cAMP		H	NH_2	MA	14.9
8-OH-cAMP		H	NH_2	OH	656
2′-O−MB-cAMP[b]		H	NH_2	H	NB[e]
Rp-cAMPS[b]		H	NH_2	H	83
Sp-cAMPS[b]		H	NH_2	H	34
Sp-cAMPS-AM[b]		H	NH_2	H	B[f]
cCMP[c]					87.2
cGMP	H	NH2	O	H	44.5
1-NH_2-cGMP	NH_2	NH2	O	H	101
2′-O−Me-cGMP[b]	H	NH2	O	H	NB[e]
cIMP	H	H	O	H	140
cPMP		H	H	H	146
2-NH_2-cPMP		NH2	H	H	101
6-Cl-cPMP		H	Cl	H	103
cUMP[c]					91.9
cXMP	H	O[d]	O	H	395

[a] Ligand is the abbreviated name. 1, 2, 6, and 8 are purine ring positions. K_I is the inhibition constant when a constant concentration of 8-fluo-cAMP and HCN2/CRP is used. [b] These ligands have modified ribofuranose rings. [c] These ligands have pyrimidine rings. [d] There is a hydrogen atom bound by the 3 position nitrogen. [e] NB means negligible binding at the highest concentrations used. [f] B means that there is noticeable binding at high concentrations but not enough for a curve.

μM and SD = 28.2 μM. A total of 4 batches of protein were used to complete measurements of the ligands.

The resulting values for 17 of the 20 ligands are shown in Table 1. The first column denotes the abbreviated name of the ligand with the next four columns denoting what chemical substituent is in the 1, 2, 6, or 8 position of the purine ring (Figure 3A for positioning). Note that the 6 position stays near the same area whether it is in *syn* or *anti* conformation. What changes is the location of the 2 and 8 substituents. The 2 position lies to the right of the ribofuranose, and the 8 position lies over the ribofuranose in the *anti* conformation (left). The 2 position lies over the ribofuranose with the 8 position to the right of the ribofuranose in the *syn* conformation (right). Substituents in the 8 position typically force the ligand into a *syn* conformation, given the steric hindrance of the position with the ribofuranose. This is not true of 2 substituents where there is no steric collision and there may even be some positive interaction with the ribofuranose.

All ligands had sufficiently complete inhibition curves to have their IC_{50}, and therefore their K_i, determined except for 2′-O-MB-cAMP, 2′-Me-cGMP, and Sp-cAMPS-AM, all ribofuranose substituted ligands. There was difficulty in obtaining complete curves for the two ligands, Sp-cAMPS-AM and 2′-Me-cGMP. Only 50% and 25% of the curves, respectively were complete. The data suggest that 1 mM might be the reliable limit for the determination of K_i using this assay. Note that two of the ligands were pyrimidine rings, cCMP and cUMP, binding with K_i values only slightly higher than that of the native ligand cAMP. cGMP binds slightly better than cAMP.

The 13 purine ring substituted ligands were divided into groups in order to make sense of the data (Figure 3B). Cyclic AMP is in the center, and each double headed arrow points to a ligand with a single substituent change. For example,

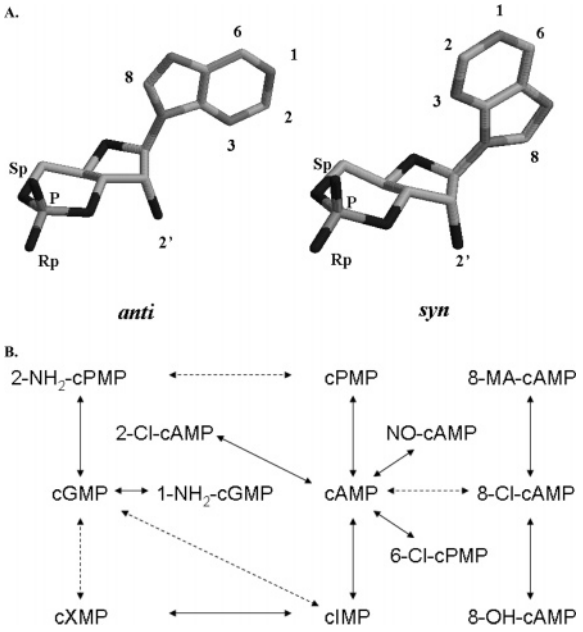

FIGURE 3: Relationship between different purine rings. (A) This is a cyclic nucleotide in *anti* (left) and *syn* (right) configuration with the positions discussed labeled. The ligands are shown with the carbons in light gray, oxygens in black, and nitrogens in dark gray. Notice that the 6 position stays in approximately the same area and that the 2 and 8 positions switch approximate steric space, the 2 position lying over the ribofuranose in *syn* conformation and the 8 position in *anti* conformation. See Table 1 for the substituent located in each position for a given ligand. (B) The purine ring analogues are shown here with the single substituent change. The ligands used to test the purine ring 2 position are to the left, those to test the 1,6 position are in the middle, and those for the 8 position are to the right. A dashed line denotes a likely conformational change in purine ring conformation. Solid lines denote related purine rings that likely do not undergo conformational change. The changes denote heavy atom changes and not hydrogen changes or bond distribution. Only one heavy atom changes from point to point.

Table 2: Relative Binding Preference Compared to those of Hydrogen or the Native Atom in Each Ligand Position[a]

	1	2	6	8
Cl		0.60	0.79	0.31
NH_2	1.23	0.41	0.43	0.26[b]
O	8.05	8.88	1.04	6.19

[a] Ligands with a single position difference were compared. The average was taken when more than one set of ligands could be used. [b] 8-MA-cAMP was used to get NH_2 for the 8 position.

the arrow between cPMP and cAMP denotes the gain of cAMP's 6 amino group to cPMP's purine ring. The dashed lines denote likely conformational changes of the ligand. Beginning with cPMP with hydrogen in positions 2, 6, and 8, the K_i of each position and its effect on ligand binding may be compared (Table 2). For example, the addition of the 6 amino group increases the binding affinity by 0.43. The addition of oxygen to cIMP (1 = H, 2 = H, 6 = O) in C^2 makes cXMP, resulting in a decrease of binding affinity by a factor of 8.88.

The values less than one denote higher affinity binding, whereas the numbers greater than one denote lower affinity binding. In this way, we have cataloged any potential ligand using the functional groups O, Cl, and NH_2 relative to hydrogen for a purine ring binding to the HCN2 binding domain. The preference rank order for each purine ring

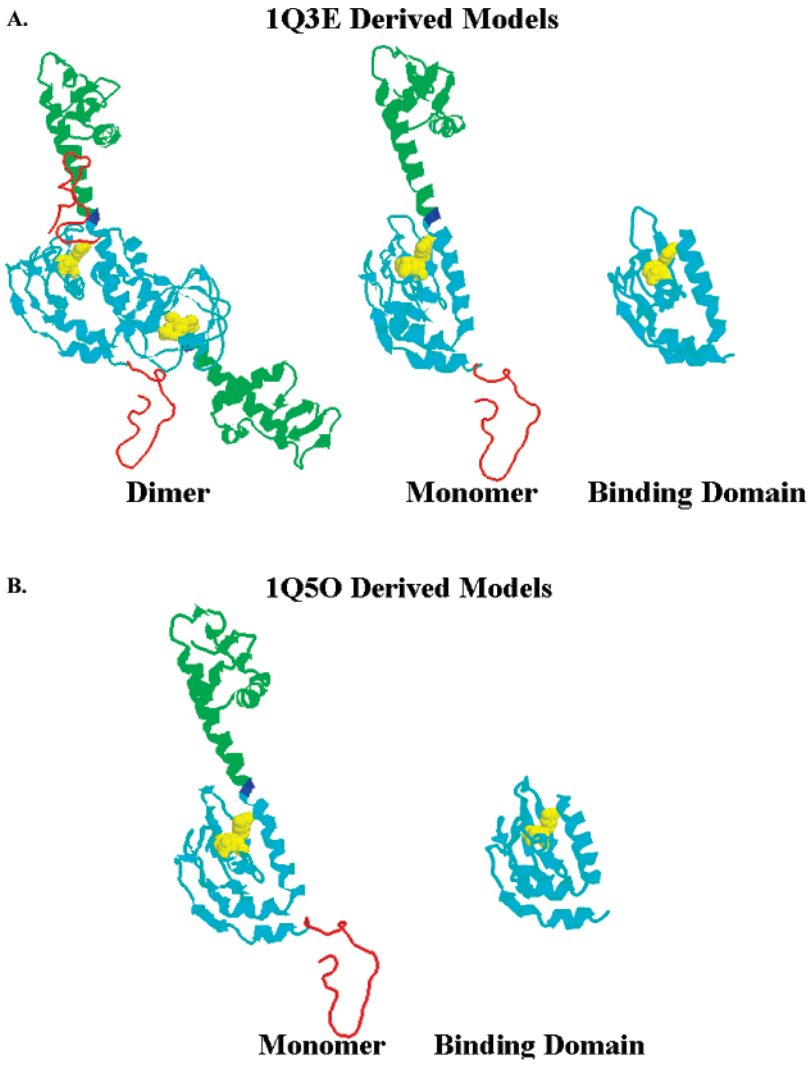

FIGURE 4: Molecular models of HCN2/CRP. (A) Molecular models based on the crystal structure 1Q3E. The left panel is an example of the dimer with the original coordinates (cyan), the added His·Tag (red), the Ala mutation (blue), and the added DNA binding domain (green). This model was also explored as a monomer (middle panel) and as the minimal binding domain (right panel). All these models show *syn*-GMP (yellow). (B) Molecular models based on the crystal structure 1Q5O. The structure was used in a monomer model (left panel) and as a minimal binding domain model (right panel). The color scheme is as described in A.

position to be determined was as follows: position 1, H > NH_2 > O; position 2, NH_2 > Cl > H > O; position 6, NH_2 > Cl > H > O; and position 8, NH_2 > Cl > H > O. Changes to ribofuranose generally result in lower affinity binding with the exception of Sp sulfur substituting for oxygen.

Molecular Modeling of the HCN2/CRP Construct. The goal of molecular modeling was to gain insight into the interactions necessary for ligand binding and to understand the binding characteristics shown in Table 2. A series of molecular models was made for each purine ring ligand on the basis of the crystal structures of HCN2 with cAMP (1Q5O) and with cGMP (1Q3E) from the pdb database using the program AMMP. The models lacked crystallographic or other water molecules. All models were minimized until a limit was reached.

The file 1Q3E bound a *syn*-cGMP and was thought to best represent the C α-helix position for molecules in the *syn* conformation. Three of these models were based on the cGMP crystal structure. The structure is a dimer with the dimerization region along the C α-helix; therefore, the first series of models were produced to explore any interactions different from the crystal structure and to see if the dimer shows unique interactions compared to those of the monomer (Figure 4A, left panel). The model was composed of coordinates from the crystal structure (ligand, yellow, and cyan ribbon), coordinates of added DNA binding domain (green), and coordinates of the added His·Tag (red). No unique long range interactions were found in the dimer. We then looked at the monomer (middle panel, colors as in the dimer) and again found no unique long range interactions. The model of the binding domain alone (right panel) showed the expected interactions noted previously in the crystal structure (*10*). Briefly, the main interactions that could be expected are a charge−charge interaction between the ribfuranose and Arg 591, interactions by the ribofuranose with additional residues Glu 582 and Thr 592, and purine ring interactions with Thr 592, Arg 632, and the hydrophobic pocket represented by Val 564, Met 572, and Ile 636. Not all of the purine ring interactions were available to *syn* ligands because Arg 632 was mediated by water in the crystal structure. Not all ligands in both conformations showed all these interactions, but they were the interactions sought and explored by the modeling. It was assumed that *syn* conformation ligands would be preferred in the 1Q3E series of

models. An analysis of the models did not support this assumption because both *syn* and *anti* conformation ligands were equally likely in these models.

The 1Q5O structure was chosen because it bound cAMP in the *anti* conformation, and the C α-helix positioned in relation to the eight-stranded β-barrel differed from that in 1Q3E. Two models were based on the cAMP bound crystal structure (1Q5O). A series of dimer models was not attempted because the crystal structure contains only a monomer and the symmetry mates of the monomer have no connections through the cyclic nucleotide binding domain. The first series of 1Q5O models contained the whole HCN2/CRP monomer (Figure 4B, left panel; the coloring scheme is as described above), and these showed no unique long range interactions. The final series of models were based on the cyclic nucleotide binding domain and showed the same groups of interactions as those described above. Again, it was believed that the *anti* conformation of ligands would be preferred here, and again this was not supported by numeric analysis.

Ligands were modeled in the *syn* and *anti* conformations in each model in an attempt to calculate which conformation was preferred as studied previously. When the five models where combined, only cGMP showed a preference for being in the *syn* conformation. The remainder of the purine ring ligands showed no preference because these had calculated energy differences between *syn* and *anti* conformations being less than 2 kJ/mol (*29*). Furthermore, there seemed to be no correspondence between the interaction energy and the binding order of ligand. For example, the interaction energies of the models for 2′-O-MB-cAMP (−129 kJ/mol average interaction energy) and 2′-O-Me-cGMP (−114 kJ/mol) consistently interacted better than cAMP (−110 kJ/mol) or cGMP (−107 kJ/mol), even though the construct had minimal affinity for 2′-O-MB-cAMP and 2′-O-Me-cGMP.

The models containing only the binding domain are used to describe interactions. The eight-stranded β-barrel is preceded by a single α-helix and followed by two α-helices. Three amino acids are shown in each Figure for orientation, Met 572 and Glu 582 in the β-barrel and Arg 632 on the final α-helix of the binding domain. The first model (Figure 5A and B) shows the *anti* purine ring of 6 Cl-cPMP between the β-barrel and C α-helix. Again, there are stacking interactions with the purine ring, but the Cl^6 is unable to interact with the backbone oxygen of Arg 632, an interaction that occurs with bound cAMP. A different orientation (Figure 5C) shows the interaction that occurs in the crystal structure between *syn*-cGMP and the Thr 592 side chain oxygen. In this Figure (Figure 5D), the O^2 of *syn*-cXMP is unable to attain the same interaction as that of cGMP's NH_2 substituent, forcing the oxygen to face away from the ligand. The O^6 interacts differently with Met 572 than *anti*-cAMP because of the differences in purine ring conformation and steric positioning. Met 572 now interacts with the electron dense oxygen instead of the electron dense purine ring. Arg 632 is still able to attain stacking interactions with the purine ring and interact with Glu 582. This model does not represent a structure that likely occurs in nature because of unfavorable interactions that would occur between the ligand and Thr 592. In a third orientation (Figure 5E and F), the Glu 582 and Arg 632 charge−charge interaction can be seen in relation to the nearby *syn* 8 position of the purine ring of 8-MA-cAMP. The 8 position lies near the hydrophobic pocket represented by Leu 574 on the β-barrel and the charge−charge interaction of Glu 582 on the β-barrel and Arg 632 on the C α-helix.

Determination of Ligand Conformation. Earlier work suggested that ligand conformation could be predicted on the basis of molecular models for the related CNGC binding domain (*29*). This suggests that before looking at models and predicting what residues may interact with the bound ligand, we must first divide the ligands into *syn* and *anti* conformations. In *syn* and *anti* conformations, the 6 position is nearly in the same position with the 2 and 8 positions swapping general regions depending on the conformation (Figure 3A). There is a nearly complete or complete conjugated ring system in all of the purine substituents, although the partially double bond oxygen can break this down. This is especially true of cXMP with two double bonded oxygens, causing the ring system to be less planar than with other substituents.

The following assumptions were used to decide what conformation a ligand would likely be in when bound to the HCN binding domain. First, any ligand would prefer the *anti* conformation because this conformation is preferred by cAMP in solution. Second, a positive interaction between the 2 position with a positive partial charge and the Sp position would cause the *syn* conformation to be more desirable as seen with cGMP in solution. Finally, any substituent in the 8 position would cause the ring to be in *syn* conformation, as occurs in solution (*30*). The additions to the ribofuranose would not effect the purine ring conformation, and therefore, the conformation would be that of the parent, *syn* for cGMP and *anti* for cAMP derivatives. Therefore, the purine ring is assumed to be in the *anti* conformation unless a partial positive charge exists in the 2 position, or there is a substituent in the 8 position. It is further assumed that the purine ring conformation would not change conformation upon binding to the HCN2 binding domain, and to our knowledge, there is no experimental evidence that a purine ring has changed conformation upon binding to this class of cyclic nucleotide binding domain.

Alterations of the N^1 Position. The N^1 position lies near the hydrophobic pocket in the *anti* conformation (Figure 5B) or in the hydrophobic pocket and near the Arg 632 oxygen in the *syn* conformation (Figure 5D). The addition of a second polar region that cannot be balanced by the backbone oxygen of Arg 632 likely leaves a highly polar group in the middle of the hydrophobic pocket. The result of this is reduced binding of the N^1 amino group or oxygen of 1.23 and 8.05, respectively. The reason for the decreased affinity of oxygen is likely due to it's proximity to the hydrophobic pocket in the parent's cAMP *anti* configuration. The parent of the amino group, cGMP, is in the *syn* conformation, placing the amino group near the Arg 632 backbone oxygen with the possibility of an interaction occurring between the two.

Alterations of the C^2 Position. The replacement of hydrogen with a neutral or positively partial charged substituent leads to a higher affinity of 0.60 and 0.41, respectively. The placing of a negative partial charged oxygen substituent reduces the binding by 8.88 times. The molecular models suggest that the reason for this binding pattern is that in the *syn* conformation the 2 position is near Thr 592

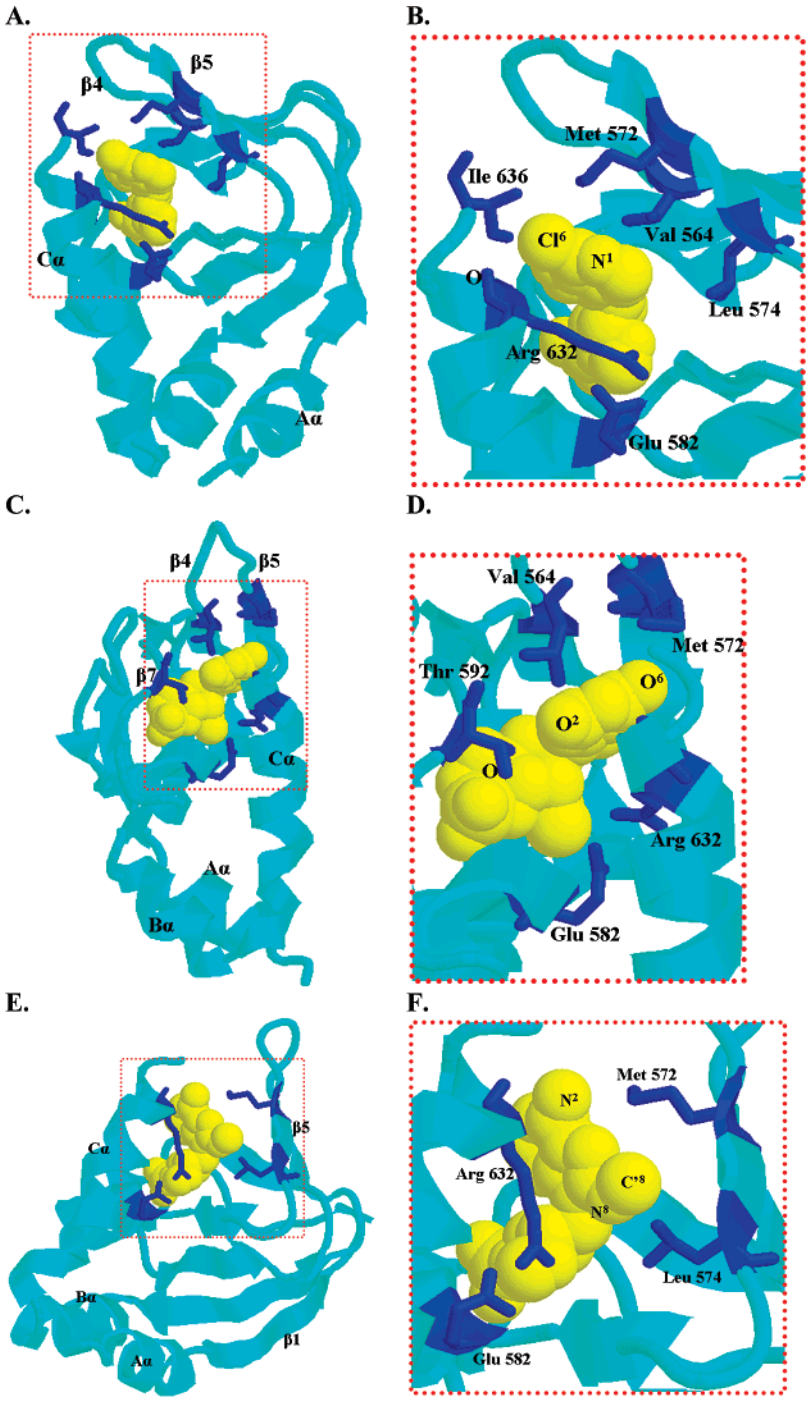

FIGURE 5: HCN2 binding domain models from different views. (A) 6-Cl-cPMP in the *anti* conformation viewed from the C^6 position. Molecular model of 6-Cl-cPMP (yellow) based on the pdb file 1Q5O. Secondary structure elements are labeled for orientation, either as β-sheet (β) or as α-helix (α). The associated number (β) or letter (α) corresponds with structural elements in Figure 1 and typical cyclic nucleotide binding domain nomenclature. The view of the ligand and selected residues (blue) is expanded in the dotted box in B. (B) Selected amino acids that surround the ligand are shown from the C6 position, which has chloride (Cl^6) attached. The Cl can no longer interact with the Arg 632 backbone oxygen as cAMP's amino group did, nor does it disrupt the stacking interactions of Arg632. The hydrophobic interactions with the purine ring are represented by Val 564, Met 572, and Leu574 throughout these figures. (C) A *syn*-XMP 1Q3E based model as viewed from the C^2 position. A close-up view of the model is seen in D represented by the dotted box. (D) The close up shows the reason cXMP is likely in the *anti* conformation. The *syn* conformation would force the Thr 592 oxygen that interacts with bound cGMP's amino group away from the ligand in an unfavorable interaction. Glu 582 interacts in a charge−charge interaction with Arg 632, which also stacks with the purine ring. O^6 is shown for the orientation of the purine ring. (E) A *syn*-8-MA cAMP 1Q3E based model as viewed from the C^8 position. The view of the dotted box is expanded in panel F. (F) N^8 and C'^8 represent the methylamino C^8 substituent. The N^2 substituent is shown for the orientation of the purine ring. This Figure shows that there is ample room between the hydrophobic pocket and the Glu 582-Arg 632 charge−charge interaction for large C^8 substituents. The C^8 substituent lies near the charge−charge interaction and likely can interact with it affecting Arg's stacking interaction.

(Figure 5D). The positively partial charged amino group is able to positively interact with the Thr's oxygen leading to the highest affinity in binding, 0.41. When the positive partial charge is removed and Cl is put in the position, the increased size compared to that of hydrogen seems to be enough to increase binding. This is because with this substituent, the

ligand would likely be in an *anti* conformation and in the hydrophobic pocket of the ligand. When oxygen is a C^2 substituent, the additional electron density is not capable of interacting with the Thr as NH_2 and actually inhibits the binding of ligand. This suggests that the ligand would be in the *anti* conformation also and the partially negatively charged oxygen would be in the hydrophobic pocket and possibly interact with Arg 632, disrupting stacking interactions with the purine ring and charge−charge interactions with Glu 582.

Alterations of the C^6 Position. The C^6 position is the most tolerant of the four purine ring positions of the replacement of hydrogen with a partial charge. Both chloride and the amino group have greater affinity than hydrogen alone by 0.79 and 0.43 times, respectively. The oxygen substituent binds slightly less than hydrogen alone by 1.04 times. This position interacts with the backbone oxygen of Arg 632. The amino group would interact directly with this atom and therefore binds the tightest with 0.43. The Cl^6 would benefit from the hydrophobic pocket allowing, presumably, water to bind the backbone oxygen. O^6 would need to interact with the Arg 632 oxygen via water and the hydrogen in the N^1 position. This translates to a reduced binding of 1.04 compared to that of the others. This binding is lower in affinity than hydrogen alone, showing that the steric effect of having an atom there is more important than any partial negative charges.

Alterations of the C^8 Position. Any substituent in this position would likely cause a ligand to adopt the *syn* conformation. This places the position in/near the hydrophobic pocket (represented by Met 572 and Leu 574) and the charge−charge interaction of Arg 632 and Glu 582 (Figure 5F). The hydrophobic pocket seems to like a steric substituent represented by the 0.31 binding of Cl. The region prefers an amino group even more, represented by methylamino group in our data, in this position represented by 0.26. The oxygen substituent is unfavorable in this position compared to hydrogen by 6.19. The reason could be that it may reposition Arg 632 away from Glu 582, breaking down the series of bonds interacting with the ribofuranose, thereby reducing overall binding.

Alterations to Ribofuranose. Ribofuranose is the main reason for this class of binding domains to bind ligands, as shown in many previous experiments (*31*−*34*). If the previous experiments were not enough evidence, we show that any cyclic nucleotide, purine, or pyrimidine ring is capable of binding with less than a 2-fold increase in K_i. The experiments here reinforce the importance of ribofuranose in binding with any large addition resulting in a loss of binding. The only change that is better tolerated is the change of Sp oxygen to sulfur on the phosphate, which shows an increased binding of 0.59. This effect was explored previously in a similar binding domain, and it was believed that the tilt of the whole ligand favored the interaction with Thr 592. Replacing the Rp oxygen with sulfur resulted in a reduced binding of 1.45 and was seen previously, explained as a tilt reducing the ability of the binding domain to bind the ligand (*35*).

DISCUSSION

Herein, we further increase the understanding of what the HCN2 binding domain requires for ligand binding by using a binding domain fragment of the HCN2 channel. The work is an exploration of the real affinity of the binding domain for any ligand. Previously, it was mentioned that HCN2 channels have a 10-fold greater apparent affinity for cAMP over cGMP. This result is very different from the near equivalent binding of cAMP and cGMP shown here. Thus, we believe the difference in binding and apparent affinity exhibited by the complete channel must be due to the ability of the ligand to modulate the channel and promote communication between the four subunits and not due to differences in binding.

Whereas the binding domain does not distinguish between cAMP and cGMP, the complete channel does. The complete channel reads the binding domain for information about the bound ligand and the differences in the positioning of the β 4/5 strand loop, β 6/7 strand loop, and the B/C α-helices. Therefore, we suggest that the binding domain adopts different conformations as a function of the ligand as read by the complete, functional channel. This information is transmitted throughout the channel. That is why the ligands bind with the same affinity to the binding domain fragment but have different apparent affinities in the complete channel.

Comments about 8-Fluo-cAMP. There is no physiological relevance to 8-fluo-cAMP other than as a fluorescent probe. To our knowledge, it has not been used on HCN2 channels as a ligand. It was beyond the scope of this article to perform electrophysiology experiments to determine 8-fluo-cAMP's effect on channel modulation in comparison to that of cAMP. The 8-fluo-cGMP and other 8-substituent ligands bind tightly to the rod CNGC channel, and in that case, it is thought to be due to the hydrophobic pocket around the *syn* 8-substituent position. It can be surmised that a similar situation occurs with the HCN2 binding domain.

Comments about the Construct. The construct has a DNA binding domain from CRP in addition to the HCN2 nucleotide binding domain. The main use of the DNA binding domain is to solubilize the cyclic nucleotide binding domain because its removal causes precipitation of the binding domain. A construct containing the C-linker region was not used because it does not appear to be soluble without 5 μM cAMP (*10*), which would have interfered with our binding experiments and made the analysis more complicated, especially if the submicromolar apparent affinity had held true.

Our construct is a dimer in solution, which is consistent with previous work (*10*, *12*, *21*). The dimer likely does not change, given previous work and a lack of the C-linker region. The dimer in solution could very well look like the structure modeled. What is known is that the tertiary structure provides no protection for the DNA binding domain and therefore does not take a CAP-like tertiary structure, evidence again that the modeled structure could be correct. It cannot be ruled out, however, that the interactions occur through the A α-helix as in the *M. loti* structure and not through the C α-helices as in the HCN2 crystal structure with cGMP.

This class of binding domain has been shown to bind cAMP and cGMP with similar affinities in the related cyclic nucleotide gated ion channel protein fragment (*21*) and in the structurally related CRP (*26*). That the HCN2 binding domain binds the two ligands with similar affinity is therefore not surprising. What these experiments add to the literature is the knowledge of the ability of HCN2 to bind many

different ligands without the bias of channel activation. The literature contains previous attempts to study ligands in cyclic nucleotide gated ion channels, but these were limited by an inability to separate activation and binding (*31*, *32*).

Value of Static Molecular Models. The value of static molecular models is to learn which amino acids and purine ring positions could interact. The static models show what could be occurring at a particular time in the binding domain. We assume that the binding domains are showing the important interactions because the model has been minimized to the lowest energy and is based on the crystal structure. This allows comparison of the ligand's interactions with the binding domains and allows rough assumptions to be made about what is occurring. These models were also good enough to suggest minimal, if any, long range interaction between the ligand and the subdomains outside the binding domain in the construct, including the artificial DNA binding domain, the His·Tag region, or the other binding domain. These models do not speak to the interdomain interactions that could occur when the binding domain is part of the complete channel.

The crystallographic water molecules were removed because they did not correspond in the two structures, 1Q3E and 1Q5O. Retaining the water molecules would have possibly biased the position of new atoms added by different purine ring substituents as well as the hydrogen atoms missing for the crystal structure resulting in distorted structures. Water is fluid and compensates for ligand changes in nature. Water would have had to be static in the models and forced to remain in position with high force restraints; otherwise, it would move away from the model unless all water, crystallographic and bulk water, was added. This would have been outside the scope of the modeling for this study.

The inability of the models to show correspondence between calculated and actual binding (*36*, *37*) suggests that something was not accounted for. It could be that there is a large entropic contribution (including water effects), that the hydrophobic effect is not completely well modeled, or that the actual position of the β 4/5 strand loop or the C α-helix is different. The molecular modeling best takes into account enthalpic and charge interactions. The only way to account for entropic effects would be to use dynamic models over a period of time, which again is outside the scope of this article. The position of β 4/5 and β 6/7 strand loops and the C α-helix have been shown to be highly variable in a related binding domain using NMR, pdb file 1WGP (Chikayama, E., Nameki, N., Kigawa, T., Koshiba, S., Inoue, M., Tomizawa, T., Kobayashi, N., and Yokoyama, S. (released 2004-11-28), unpublished work), showing another place for entropic effects. This suggests that the β 4/5 strand loop, β 6/7 strand loop, or the C α-helix could be in different positions for each ligand, and this positioning would affect the binding calculations.

The inability to calculate conformation or binding does not invalidate the models because they serve only as guides to suggest what interactions may occur. The models are successful in this endeavor because they show the regions that likely interact. This claim is further strengthened by the 20 NMR models that show minimal to no movement of the 8 β-barrel backbone except for the loops between β-strands 4/5 and 6/7. The rest of the β-barrel is static. The structure shows no ligand, but that would also be very fluid, able to move about the binding pocket to find the minimal energy conformation.

Hypothetical Binding Model. The cyclic nucleotide binding domain likely acts similarly, whether a part of CRP, protein kinases, CNG channels, or HCN channels. First, the eight-stranded β-barrel breathes, exposing the conserved Arg (residue 591 in HCN2) on the β 6/7 strand loop. Arg interacts with the phosphate group to seat ribofuranose into the binding pocket. The conserved Thr or Ser (Thr 592) on β7 locks the ribofuranose into position with the rest of the pocket collapsing around the ligand, including the conserved Glu (582). The ligand conformation likely does not change from the conformation in solution unless amino acid side chain interactions force the purine ring to adapt a new conformation.

The ligand's purine ring is then able to alter the position of the collapsing loop between β-strands 4/ 5 and the C α-helix. The *anti* cAMP typically causes a rotation in the C α-helix as seen in HCN2 (*10*) and proposed for CRP (*26*). The position of the C α-helix directly positions the B α-helix as it forms the fulcrum from which the C α-helix is an extension. The B α-helix in turn positions the A α-helix, which runs antiparallel. *syn*-cGMP more easily positions the β 4/5 strand loop as proposed for the bovine rod α-subunit of CNG channels (*32*), although *anti*-cAMP clearly interacts with this region also as seen in CRP (*26*). The final positioning of the β 4/5 strand loop or the B and C α-helices determines the contacts of the subdomains surrounding the binding domain and determines whether the protein is active or inactive.

Why the difference in $K_{0.5}$ and K_i for cAMP and cGMP? Can we explain the difference between the in $K_{0.5}$ and K_i for cAMP and cGMP given the hypothetical binding model? All binding measurements on binding domains from CRP (*26*), CNGC (*21*), and HCN have given results in the micromolar range. The molecular models of the three binding domains cannot account for this (*26*, *29*, *32*) because they all have the important residues for binding conserved, including Arg (HCN 591), Thr (592) or Ser, and Glu (582). It has been shown through ligands and mutagenesis that the Arg (591) interacting with the ligand's ribofuranose is the main determinant of binding for this class of binding domain. How then does this yield a sudden boost to nanomolar apparent affinity?

Static molecular models, the type shown here and those referenced, leave out an important component of binding energy, entropy. The molecular models do a good job of estimating enthalpy that comes from charges and distances but do not address entropy. Therefore, given the Arg, Thr or Ser, and Glu, one will always record similar enthalpy measurements. What can change to give better binding is the exposure of the Arg to the ligand or the breathing rate of the β 6/7 strand loop.

All of the K_d or K_i measurements on the binding domains have been done in solution with no concern for voltage gradients. The complete HCN2 channel is voltage gated and modulated by cyclic nucleotide. Hence, we propose that the reason for nanomolar $K_{0.5}$ is an entropic component derived from the channel itself, in the form of voltage. When the HCN channel experiences a voltage change, part of the energy is allocated to the ligand binding domain, which

breathes more than it normally does. The added exposure of Arg therefore leads to an increased rate of binding cyclic nucleotide. The other binding domains mentioned, CRP and CNG channels, do not have this influx of energy and therefore have reduced affinities for the ligand. This entropic mechanism is consistent with the inhibitory effect of the cyclic nucleotide binding domain on the channel as shown in experiments in which removal of the binding domain generated response curves similar to those with saturating cAMP (*38*).

This positive entropic effect is also visible in the interaction between cGMP and the binding domain. The apparent affinity of cGMP for the intact channel is 6 μM, almost an order of magnitude higher than the affinity of the binding domain alone. This means that the energetic enhancement of the complete channel experienced by cAMP is also available to cGMP. The additional apparent affinity of cAMP compared to that of cGMP is likely due to cAMP's ability to allow better communication between the binding domain and the channel, likely communicated via the C α-helix.

What emerges is a binding model where the intact channel using a voltage gradient allows cAMP to bind and communicate its presence to the channel via the nucleotide binding domain better than cGMP is able to communicate it. The reason for *anti*-cAMP's superiority as an agonist is that the intact channel reads the presence and position of the binding domain elements, the β 4/5 strand loop, β 6/7 strand loop, and the C α-helix better then it reads the positioning achieved by *syn*-cGMP. These elements must communicate with the channel gating region in a more efficient way when cAMP is bound than when cGMP is bound.

Purine Ring Interactions. Although the purine ring has been shown to affect binding, its main job is to be read by the binding domain in order to activate the protein. It is no mistake that cAMP and cGMP bind to the proteins with similar affinity but can cause marked differences in protein activation. It is the substitutents on the purine ring and their interactions with the binding domain that determine activation. The first consideration about the purine ring is the conformation it takes in the binding domain. This conformation defines the location of the substituents and the surrounding amino acids it interacts with. These interactions, positive or negative, determine whether the ligand will activate the channel. In addition, these same interactions modify the length of time a ligand will stay bound to the binding domain. The results shown here only speak to binding, and other experiments must be pursued to determine the ability of these ligands to activate the channel.

The following four purine ring positions that interact with the binding domain have been mapped here: N^1, C^2, C^6, and C^8 positions. The N^1 and C^6 positions interact with the Arg 632 backbone oxygen and Met 572 whether in the *syn* or *anti* conformation. The *syn* conformation can interact with the backbone via a water molecule as shown in the crystal structure (*10*). The C^2 position interacts with Thr 592 in the *syn* conformation and the hydrophobic pocket and Arg 632 when in the *anti* conformation. The Thr 592 interaction with cGMP is likely very important for determining that the ligand is bound. The C^8 position will interact with the hydrophobic pocket and Arg 632. If charged, this can interact with the charge−charge interaction of Glu 582 and Arg 632. Furthermore, large 8-substituents can lead to much tighter binding than expected, as seen with 8-fluo-cAMP. Similar high binding affinities have been proposed for the bovine rod α-CNG channel and the ligand 8-fluo-cGMP (*31*).

There is 93% identity between HCN2 and HCN1 cyclic nucleotide binding domains, 81% between HCN 2 and HCN 3, and 97% between HCN2 and HCN4. All of the interactions mentioned previously should be retained because only the Met 572 interaction differs in HCN3 and HCN4 being replaced by Thr. The other differences occur throughout the binding domains and likely do not affect the purine ring interactions but could affect the communication of the binding domain with other parts of the channel.

All of the purine ring interactions have correlates to those in CRP (22% identity with HCN2) and the bovine rod α-CNG channel (41% identity) cyclic nucleotide binding domains. The equivalent of Thr 592 is present in both binding domains, as Ser in CRP, and has similar interactions with the C^2 position. The Met 572 interaction has correlates also, with Ser in CRP and Phe in the bovine rod α-CNG channel. Ser is in an equivalent position, and Phe is one position higher in the highly variable β 4/5 strand loop. The Arg 632 backbone interaction with position C^6 is replaced by amino acid interactions with Thr in CRP and Asp in the bovine rod α-CNG channel. The hydrophobic pocket around C^8 is present in both CRP and the bovine rod α-CNG channel, as is the Glu−Arg charge interaction, although a Lys replaces the Arg in the bovine rod α-CNG channel. Therefore, all of the main amino acid interactions present in HCN2 are consistently present in other cyclic nucleotide binding domains. Furthermore, because the positions work in concert in these other binding domains (*39*) to determine the ability of a ligand to activate the protein, the same likely occurs in the HCN2 binding domain.

Biological Significance. How does the construct relate to the whole channel, and is it able to take on biologically relevant conformations in the absence of the rest of the channel? The principal assumption of this work is that fragments of the channel will work in the absence of the rest of the channel. Therefore, we believe that the construct takes on the biologically relevant conformation when the ligand binds, with much of the β-barrel remaining static while the β 4/5 and 6/7 strand loops and C α-helix collapse on the ligand as it is bound as described above. These motions occur in the complete, functional channel but are influenced by other regions and subunits.

Again, as previously stated, the channel likely contributes to the binding domain becoming more receptive to the ligand in order to account for the higher than expected apparent affinity. The results here show the ability of a well folded fragment of the channel to bind ligands in the absence of the rest of the channel. The results here state that certain purine ring substituents are preferred in the N^1, C^2, C^6, and C^8 positions with the following rank order: position 1, H > NH_2 > O; position 2, NH_2 > Cl > H > O; position 6, NH_2 > Cl > H > O; and position 8, NH_2 > Cl > H > O. The binding rank order may change in the complete channel, but this is unlikely because the channel relies on the binding domain to determine what is on the purine ring. This does not say that the activation rank order has to be the same, and it likely is different.

The rest of the channel can determine what it does with the information read out of the binding domain. That is why equivalent interactions in the binding domain can lead to very different results. For example, the HCN 1 and 2 binding domains are the same in the purine ring contact residues yet have very different responses to cAMP (*34*). This is due not to the binding domain but to the way in which the rest of the channel responds to the information received from the binding domain. A similar rank order of ligands likely will result from a study of the HCN1 binding domain for binding. A very different response of the channel can be expected because cAMP has little response in HCN1.

The results here can be used to parse out individual interactions and be used for activities such as drug design. There are several proteins that use the binding domain motif explored here, including CNG channels, the various cyclic nucleotide dependent kinases, and HCN subtypes. By determining the rank order of binding to these binding domains, we can determine which modified ligands might prefer certain binding domains. This information, along with functional studies of the complete protein, can be used to determine whether possible drug targets will have the desired effect and, more importantly, whether they will have a cross effect on a protein with a similar binding domain.

In summary, we have developed a fluorescent binding assay for the HCN2 binding domain that can determine binding domain kinetics independent of channel activation. The assay can be used to rapidly determine which ligands are capable of binding to the binding domain, even though they may not alter channel currents. Furthermore, ligand modifications can be rapidly assessed as to their effect on channel binding, effectively mapping important interactions between the ligand and the binding domain. We used molecular models to visualize and interpret the possible interactions that occur to suggest a way in which the binding domain may select for certain substituents in each purine ring position. Finally, this assay should be adaptable to other soluble constructs to define binding and ligand interactions with other cyclic nucleotide binding domains.

ACKNOWLEDGMENT

We thank Dr. Richard Willson in the Department of Chemical & Biomolecular Engineering and Biology & Biochemistry at the University of Houston for the use of his fluorometer. We also thank Dr. Joseph Jez at Donald Danforth Plant Science Center for determining the multimerization state of HCN2/CRP using HPLC. We thank Dhasakumar Navaratnam in the Department of Neurology and Neurobiology at Yale University School of Medicine for his gift of HCN2 binding domain cDNA.

REFERENCES

1. Colquhoun, D. (1998) Binding, gating, affinity, and efficacy: the interpretation of structure-activity relationships for agonists and of the effects of mutating receptors, *Br. J. Pharmacol. 125*, 923−947.
2. Noma, A., and Irisawa, H. (1976) Membrane currents in the rabbit sinoatrial node cell as studied by the double microelectrode method, *Pflügers Arch. 364*, 45−52.
3. Brown, H. F., DiFrancesco, D., and Noble, S. J. (1979) How does adrenaline accelerate the heart? *Nature 280*, 235−236.
4. Halliwell, J. V., and Adams, P. R. (1982) Voltage-clamp analysis of muscarinic excitation in hippocampal neurons, *Brain Res. 250*, 71−92.
5. Bader, C. R., Macleish, P. R., and Schwartz, E. A. (1979) A voltage-clamp study of the light response in solitary rods of the tiger salamander, *J. Physiol. 296*, 1−26.
6. Robinson, R. B., and Siegalbaum, S. A. (2003) Hyperpolarization-activated cation currents: from molecules to physiological function, *Annu. Rev. Physiol. 65*, 453−480.
7. Santoro, B., Liu, D. T., Yao, H., Bartsch, D., Kandel, E. R., Siegelbaum, S. A., and Tibbs, G. R. (1998) Identification of a gene encoding a hyperpolarization-activated pacemaker channel of brain, *Cell 93*, 717−729.
8. Ludwig, A., Zong, X., Jeglitsch, M., Hofmann, F., and Biel, M. (1998) A family of hyperpolarization-activated mammalian cation channels, *Nature 393*, 587−591.
9. Craven, K. B., and Zagotta, W. N. (2005) CNG and HCN channels: two peas, one pod, *Annu. Rev. Physiol. 68*, 375−401.
10. Zagotta, W. N., Olivier, N. B., Black, K. D., Young, E. C., Olson, R., and Gouaux, E. (2003) Structural basis for modulation and agonist specificity of HCN pacemaker channels, *Nature 425*, 200−205.
11. Hua, L., and Gordon, S. E. (2005) Functional interactions between A′ helices in the C-linker of open CNG channels, *J. Gen. Physiol. 125*, 335−344.
12. Clayton, G. M., Silverman, W. R., Heginbotham, L., and Morais-Cabral, J. H. (2004) Structural basis of ligand activation in a cyclic nucleotide regulated potassium channel, *Cell 119*, 615−627.
13. Anderson, W. B., Schneider, A. B., Emmer, M., Perlman, R. L., and Pastan, I. (1971) Purification of and properties of the cyclic adenosine 3′,5′-monophosphate receptor protein which mediates cyclic adenosine 3′,5′-monophosphate-dependent gene transcription in *E. coli*, *J. Biol. Chem. 246*, 5929−5937.
14. Aiba, H., Fujimoto, S., and Ozaki, N. (1982) Molecular cloning and nucleotide sequencing of the gene for *E. coli* cAMP receptor protein, *Nucleic Acids Res. 10*, 1345−1361.
15. Cossart, P., Gicquel-Sanzey, B., and Adhya, S. (1982) Cloning and sequence of the crp gene of *E. coli* K 12, *Nucleic Acids Res. 10*, 1363−1378.
16. Anderson, W. B., Perlman, R. L., and Pastan, I. (1972) Effect of adenosine 3′,5′-monophosphate analogues on the activity of the cyclic adenosine 3′,5′-monophosphate receptor in *Escherichia coli*, *J. Biol. Chem. 247*, 2717−2722.
17. McKay, D. B., Weber, I. T., and Steitz, T. A. (1982) Structure of catabolite gene activator protein at 2.9 Å resolution, *J. Biol. Chem. 257*, 9518.
18. Weber, I. T., Steitz, T. A., Bubis, J., and Taylor, S. S. (1987) Predicted structures of cAMP binding domains type I and II regulatory subunits of cAMP dependent protein kinase, *Biochemistry 26*, 343−351.
19. Harrison, R. W., Chatterjee, D., and Weber, I. T. (1995) Analysis of six protein structures predicted by comparative modeling techniques, *Proteins 23*, 463−471.
20. Belduz, A. O., Lee, E. J., and Harman, J. G. (1993) Mutagenesis of the cyclic AMP receptor protein of *Escherichia coli*: targeting positions 72 and 82 of the cyclic nucleotide binding pocket, *Nucleic Acids Res. 21*, 1827−1835.
21. Scott, S.-P., Weber, I. T., Harrison, R. W., Carey, J., and Tanaka, J. C. (2001) A functioning chimera of the cyclic nucleotide-binding domain from the bovine retinal rod ion channel and the DNA-binding domain from catabolite gene-activating protein, *Biochemistry 40*, 7464−7473.
22. Horton, R. M., Ho, S. N., Pullen, J. K., Hunt, H. D., Cai, Z., and Pease, L. R. (1993) Gene splicing by overlap extension, *Methods Enzymol. 217*, 271−279.
23. Nikolovska-Coleska, Z., Wang, R., Fang, X., Pan, H., Tomita, Y., Li, P., Roller, P. P., Krajewski, K., Saito, N. G., Stuckey, J. A., and Wang, S. (2004) Development and optimization of a binding assay for the XIAP BIR3 domain using fluorescence polarization, *Anal. Biochem. 332*, 261−273.
24. Weber, I. T., and Steitz, T. A. (1987) Structure of a complex of catabolite gene activator protein and cyclic AMP refined at 2.5 Å resolution, *J. Mol. Biol. 198*, 311−326.
25. Passner, J. M., Schulz, S. C., and Steitz, T. A. (2000) Modeling the cAMP-induced allosteric transition using the crystal structure of CAP-cAMP at 2.1 Å resolution, *J. Mol. Biol. 304*, 847−859.
26. Scott, S.-P., and Jarjous, S. (2005) Proposed structural mechanism of *Escherichia coli* cAMP receptor protein cAMP-dependent proteolytic cleavage protection and selective and nonselective DNA binding, *Biochemistry 44*, 8730−8748.

27. Harrison, R. W. (1993) Stiffness and energy conservation in the molecular dynamics: an improved integrator, *J. Comput. Chem. 14*, 1112−1122.
28. Hofmann, F., Biel, M., and Kaupp, U. B. (2005) International Union of Pharmacology. LI. Nomenclature and structure-function relationships of cyclic nucleotide-regulated channels, *Pharmacol. Rev. 57*, 455−462.
29. Scott, S.-P., Harrison, R. W., Weber, I. T., and Tanaka, J. C. (1996) Predicted ligand interactions for 3′,5′-cyclic nucleotide-gated channel binding sites: comparison of retina and olfactory binding site models, *Protein Eng. 9*, 333−344.
30. Stolarski, R., Dudycz, L., and Shugar, D. (1980) NMR studies on the syn-anti equilibrium in purine nucleosides and nucleotides with the aid of 1H and 13C NMR, *Eur. J. Biochem. 108*, 111−121.
31. Tanaka, J. C., Eccleston, J. F., and Furman, R. E. (1998) Photoreceptor channel activation by nucleotide derivatives, *Biochemistry 28*, 2776−2784.
32. Scott, S.-P., and Tanaka, J. C. (1995) Molecular interactions of 3′,5′-cyclic purine analogues with the binding site of retinal rod ion channels, *Biochemistry 34*, 2338−2347.
33. Tibbs, G. R., Liu, D. T., Leypold, B. G., and Siegelbaum, S. A. (1998) A state-independent interaction between ligand and a conserved arginine residue in cyclic nucleotide-gated channels reveals a functional polarity of the cyclic nucleotide binding site, *J. Biol. Chem. 273*, 4497−4505.
34. Chen, S., Wang, J., and Siegalbaum, S. A. (2001) Properties of hyperpolarization-activated pacemaker current defined by Co assembly of HCN1 and HCN2 subunits and basal modulation by cyclic nucleotide, *J. Gen. Physiol. 117*, 491−503.
35. Scott, S.-P., Cummings, J., Joe, J. C., and Tanaka, J. C. (2000) Mutating three residues in the bovine rod cyclic nucleotide-activated channel can switch a nucleotide from inactive to active, *Biophys. J. 78*, 2321−2333.
36. Harrison, R. W., and Weber, I. T. (1994) Molecular dynamics simulation of HIV-1 protease with peptide substrate, *Protein Eng. 7*, 359−369.
37. Xu, L. Z., Weber, I. T., Harrison, R. W., Gidh-Jain, M., and Pilkis, S. J. (1995) Sugar specificity of human B-cell glucokinase: correlation of molecular models with kinetic measurements, *Biochemistry 34*, 6083−6092.
38. Wainger, B. J., DeGennaro, M., Santoro, B., Siegelbaum, S. A., and Tibbs, G. R. (2001) Molecular mechanism of cAMP modulation of HCN pacemaker channels, *Nature 411*, 805−810.
39. Scott, S.-P., and Tanaka, J. C. (1998) Three residues predicted by molecular modeling to interact with the purine moiety alter ligand binding and channel gating, *Biochemistry 37*, 17239−17252.

BI6026049